International Journal of Environmental Sciences
ISSN: 2229-7359
Vol. 11 No. 2, 2025
https://www.theaspd.com/ijes.php

Optimizing PLGA Nanobubbles For Triggered Enzalutamide Delivery: Preparation, Characterization, And Evaluation Using Design Of Experiments

Narendra Kundavarapu[*1], Kannadasan Mahalingam[2], Kiran Kumar Y[3]
[1]Research Scholar, Faculty of Pharmaceutical Sciences, Motherhood University, Roorkee, Uttarakhand – 247661. India.
[2]Professor & Principal, Faculty of Pharmaceutical Sciences, Motherhood University, Roorkee, Uttarakhand – 247661. India
[3]Gate Institute of Pharmaceutical Sciences, Chilkuru, Suryapet, 508206, Telangana, India

Abstract
Enzalutamide (ENZ) serves as an androgen receptor signaling inhibitor, is used to treat prostate cancer, and has received approval from the US FDA. ENZ pharmaceutical applications are hindered due to low solubility, first-pass metabolism, and limited bioavailability. This research aimed to develop and optimize polylactic acid co-glycolic acid (PLGA) nanobubbles as a sustained delivery system for ENZ, improving stability and bioavailability. Through a three-factor, three-level Box Behnken Design, 17 experimental runs were carried out to optimize drug-PLGA nanobubbles. The optimized formulation consisted of a 40 mg drug, 250 mg PLGA, and 1.9% w/v polyvinyl alcohol (PVA)as a stabilizer. The nanobubbles displayed a particle size of 193.5 ± 2.8 nm, polydispersity index of 0.26 ± 0.016, and zeta potential of 31.4 ± 1.17 mV, with an entrapment efficiency of 65.12 ± 2.54%.Analysis through Fourier transform infrared spectroscopy, differential scanning calorimetry, and X-ray diffraction confirmed no drug-polymer interaction while scanning electron microscopy revealed uniform spherical nanoparticles. In vitro studies exhibited excellent drug release, and stability studies showed no significant changes after one month. In vivo studies in rats demonstrated increased Cmax (6.84) and AUC0-t (5.874), indicating improved sustained release and absorption. The findings highlight the potential of ENZ-loaded PLGA nanobubbles to enhance drug kinetics and bioavailability, opening possibilities for precise delivery and improved therapeutic effectiveness. This study provides valuable insights into the variables that impact oral absorption in nanobubble formulations, which can inform future strategies for developing oral drugs.
Keywords: *Box-Behnken design, Enzalutamide, Nanobubbles, PLGA*

1. INTRODUCTION

Globally, prostate cancer is a widespread concern, with around 1.4 million new cases reported in 2020. Prostate cancer ranks as the 2nd most prevalent form of cancer and stands as the fifth primary contributor to cancer-related fatalities in men across the globe1. In India, prostate cancer is also a significant health issue, accounting for a significant proportion of cancer cases in men. The occurrence of prostate cancer in Asian countries have been increasing in recent years, primarily related with the aging population and changing lifestyles2. However, awareness and screening programs in India are still in the early stages of development, highlighting the need for increased efforts in prevention, early detection, and access to high-quality care to alleviate the burden of prostate cancer in the country. Androgen deprivation therapy (ADT) is a well-established treatment strategy for locally advanced and metastatic prostate cancer (PC), providing relief from symptoms and producing positive biochemical and objective responses3. Prior to 2012, nonsteroidal antiandrogen drugs like bicalutamide and flutamide were commonly utilized but proved ineffective as the cancer progressed to a hormone-refractory stage4. However, since 2012, the introduction of novel second-generation antiandrogen drugs such as Enzalutamide (ENZ) and Apalutamide (APL) has brought about new possibilities in the treatment of castration-resistant prostate cancer (CRPC), addressing the limitations of previous therapies5. Enzalutamide (ENZ) serves as an androgen receptor signaling inhibitor, effectively halting the proliferation of prostate cancer cells and inducing their apoptosis. By explicitly targeting androgen receptor signaling pathways, ENZ suppresses cancer cell growth and triggers their programmed cell death. This dual action highlights the efficacy of ENZ in treating prostate cancer and

underscores its potential as a valuable therapeutic tool in combating this disease6–8.ENZ received approval from the U.S. Food and Drug Administration (FDA) in the year 2012 for the treatment of metastatic CRPC, and apalutamide was approved for treating non-metastatic CRPC in 20189,10. ENZ is classified as BCS class II owing to its high permeability and low solubility in water(0.00136 mg/mL), with a log p of 3.75 and melting point of 201℃ 9.The chemical formula is C21H16F4N4O2S. The bioavailability of the drug is only 1 percent. Currently, the drug is available in two strengths (40 and 80 mg/p.o).The drug binds predominantly to plasma proteins, mainly albumin, with a binding rate of 97% to 98%.Despite its therapeutic potential, the drug exhibits low bioavailability, necessitating high doses for efficacy, which poses a significant limitation. Different authors have employed various approaches to improve ENZ's solubility by utilizing solid-form optimization techniques. These approaches encompass solid dispersion, nanocrystals, and the integration of polymers like polyethylene glycol 6000 (PEG), β-cyclodextrin (β-CD), and modified cyclodextrins11. Self-nano emulsifying drug delivery system (SNEDDS)12, solid SNEDDS13, and solid lipid nanoparticles (SLNs) were reported14.While various carrier systems have been explored for the delivery of ENZ, they are not without limitations. Difficulties encompass stability challenges, complications in scaling up, fluctuations in bioavailability, compatibility issues with specific medications, obstacles in meeting regulatory requirements, and increased manufacturing expenses. Despite advancements, achieving deep tissue penetration and effective drug distribution remains a challenge for some of the above approaches. Addressing these limitations through continued research and innovation is crucial to fully realize the therapeutic potential of quercetin in treating various diseases. In addition to improving solubility, it is crucial to have a method that can direct drug molecules to diseased tissues while minimizing their presence in healthy tissues. The targeted delivery system will enhance the concentration of drug in the blood while improving the pharmacokinetics of the drug while reducing the side effects. Innovative delivery systems, particularly those aimed at cancer treatment, are an example of such systems. Nanobubbles, tiny bubbles at the nanoscale, are utilized in various fields, particularly in drug delivery systems, due to their exceptional physical characteristics. They offer remarkable stability, high internal pressure, and a large surface-to-volume ratio15. Nanobubbles range in size from 500 nm to 1 nm. They may becustomized precisely using amphiphilic polymers or surfactants. While research has been conducted on polymeric and lipidic nanobubbles, lipid-based nanobubbles are less stable, resulting in a shorter circulation period16. PLGA(polylactic co-glycolic acid), an exceptional nano/micro biomaterial, is extensively utilized in various fields, including targeted drug delivery, molecular diagnostics, tissue engineering, and gene transfer. The widespread utility of PLGA can be attributed to its remarkable properties, which include exceptional stability, biodegradability, and ease of chemical modification. Numerous researchers have utilized PLGA as a polymer in producing nanobubbles for the targeted delivery, owing to its diverse benefits and suitability. To the best of our knowledge and based on the available literature, there are no prior studies documenting the utilization of PLGA nanobubbles (NBs) for delivering ENZ. This research addresses a void in the field by utilizing PLGA nanobubbles (NBs) for ENZ delivery and implementing the Design of Experiments (DoE) for enhancement. DoE simplifies optimizing experimental variables through clear-cut strategies and statistical methods. The study involves designing, formulating, and optimizing drug-loaded NBs using PLGA, followed by comprehensive in-vitro and in-vivo evaluation.

2. MATERIALS AND METHODS

Reagents and chemicals

Enzalutamide (ENZ) is a pure drug given by Dr. Reddy's Laboratories, a private limited company in Hyderabad. C3F8 (Perfluoro propane) was procured from pharm affiliates Pvt ltd, Haryana, India. Sigma Aldrich, US, supplied Poly (D, L-lactide-co-glycolide) 50:50 with an intrinsic viscosity of 0.22 dl/g and Mw 25,000. Polyvinyl alcohol (PVA; Mw 30,000-70,000) was purchased from Sigma Aldrich (St. Louis, MO, USA). Isopropanol and dichloromethane were acquired from S.D. Fine Chemicals, Hyderabad. All other solvents were purchased from Qualigens, India.

Analytical method development using RP-HPLC

Chromatographic analysis of ENZ was executed using a Shimadzu prominencemodel LC-20AD equipped

with a UV detector set at 270 nm for ENZ. Areverse phase Luna C-18 column (150 mm × 4.6 mm i.d., 5.0 µm practical size and 100 Å pore size) maintained at 40.0±0.1 °C was employed. The mobile phase is composed using a blend of ammonium acetate buffer(40mM) and acetonitrile in the ratio of 60:40(v/v) and the flow rate was adjusted to 1.5 mL/min. A standard stock solution of the drug at a concentration of 1000µg/mL was prepared, followed by the creation of various working standard solutions ranging from 0.5 to 100 µg/mL through serial dilutions. A stock solution (1000µg/mL) of nilutamide as IS (internal standard) after appropriate dilution was included in the experiment17.

Enzalutamide nanobubbles (ENZ-NBs) formulation development and optimization

Enzalutamide-loaded PLGA nanobubbles were synthesized using solvent evaporation with ultrasound assistance following a reported method with slight modifications. At first, a homogeneous solution was formed by dissolving PLGA (200 mg) in a water-immiscible solvent, dichloromethane (DCM). The drug (ENZ) was then added to create a dispersion, which underwent sonication for five minutes at 45% amplitude in an ice bath using a Digital Sonifier S-250D (Branson Ultrasonic, Danbury, USA). Next, the drug dispersion was combined with 25 mL of chilled 1.9 % PVA (polyvinyl alcohol) solution and homogenized at 12200 rpm for 12 minutes using a high-speed homogenizer. The formulation was then subjected to sonication using an ultrasonic probe at 30 W for 3 minutes. A 2.5% v/v isopropanol solution (25 mL) was added to the emulsion and mechanically stirred for 5 hours to remove the dichloromethane. After that, the resulting product was centrifuged for five minutes at 8000 rpm. The product was washed with distilled water after discarding the supernatant. This centrifugation and washing process was repeated three times. The nanobubbles were freeze-dried without light for 36 h using a LYPH LOCK 4.5 (Labconcocorporation, Kansas city). Later, C3F8 gas (perfluoropropane) was added to the lyophilization chamber through a vial connector at a flow level of 50 mL/min for 1 minute. After this, the screw vials were tightly sealed for further analysis18. ENZ-loaded PLGAnanobubble optimization was achieved by implementing a three-factor, three-level BBD.A total of 17 experimental runs, including three replicated center points 19. The three independent variables were the amount of PVA (w/v) homogenization speed (rpm) and homogenization time, each at three levels of variation: low (-1), middle (0), and high (1). The response (four dependent variables) was particle size (Y1), polydispersity index (PdI)(Y2), zeta potential (Y3), and encapsulation efficiency (EE%) (Y4); Table 1 lists their respective ranges. Utilizing response surface charts and contour (2D) plots, the response surface search was carried out with Design Expert® tools (Version 12.0.3.0, Stat-Ease Inc., Minneapolis, MN).

Table 1: Factors influencing the experiment's design

		Levels		
	Independent variables	LOW (-1)	Medium (0)	High (+1)
A	Amount of PVA (% w/v)	1.0	1.5	2.0
B	Homogenization speed(rpm)	10000	12500	15000
C	Homogenization time(mins)	5	10	15
Dependent variables		*Restrictions*		
Y1	Particle size (nm)	Minimize		
Y2	Polydispersity index	Minimize		
Y3	Zeta potential (mV)	Maximum		

Y4	Encapsulation Efficiency (%)	Maximum

CHARACTERIZATION AND EVALUATION

Measurements of PS, PdI, and ZP

Using a Zetasizer (Malvern Instruments, UK), DLS theory (dynamic light scattering) was used to calculate the PS,PdI, and ZP of ENZ NBs after tenfold dilution of the sample with double-distilled water[19].

Entrapment efficiency (EE)

The EE of the drug in the nanobubbles can influence the therapeutic efficacy, stability, and release kinetics of the loaded compounds within the nanobubbles. Dichloromethane was used to dissolve a particular quantity of loaded drug (ENZ)-containing NBs. The complex was dissolved by subjecting the solution to sonication for 10 minutes.The resultant solution was then suitably diluted and assessed for the using the above-mentioned HPLC method.

The following formulae can be used to calculate the same.

$$\%\ Drug\ Entrapment\ efficiency\ = \frac{Total\ amount\ of\ the\ drug - free\ drug}{amount\ of\ drug} \times\ 100$$

Morphology using Scanning electron microscopy (SEM)

Using a Quanta FESEM 250 SEM, the structure of the nanobubbles and drug was captured. Before testing, the sample was mounted on aluminum pin stubs after being double-sided carbon tape-mounted and Au-sputter coated utilizing an ion splutter. The specimen was then analyzed at an operating distance of 10 millimeters, with an acceleration current of 30 kV and a magnification of 500–10,000 folds[20].

Fourier-Transform Infrared (FTIR) Spectroscopy

The spectrum of FTIR was obtained using spectroscopy Perkin Elmer (Model 1600; USA). The pure drug, PLGA, physical mixture (PM), and the optimized drug-loaded NBs were all analyzed at wave numbers 4000-450 cm^{-1} with a resolution of 1.0 cm^{-1}[21].

Differential Scanning Calorimetric study and X-ray diffraction pattern (XRD)

DSC (DSC-60, Shimadzu Corp., Japan) was employed to ascertain the drug's physical structure and the potential for chemical interactions with the excipients. Samples of 3-5 mg (pure drug, blank NBs, PLGA, optimized drug loaded NBs, and NBs stored for three months) were subjected to heating (50-400 °C, 5 °C/min) in folded aluminum pans in a nitrogen environment before being subjected to DSC analysis following calibration using Indium and lead standards. The melting point (MP) and the enthalpy of fusion were computed automatically. The X-ray diffraction patterns of pure drug, physical mixture, and the optimized formulations were obtained using a Philips X-ray diffractometer (PW-1710) operational with a graphite monochromator and Ni-filtered Cu Kα radiation (at 100mV and 40kV).The samples were scanned between 2 and 80 degrees 2 theta (θ) angle from 2° to 60° with an average step size of 0.045° and a duration per step of 0.5 seconds[13].

Drug release (DR)

The release studies of (PD) pure drug and optimized drug-loaded PLGA NBs were carried out through in vitro experiments using a shake flask equipped with a dialysis bag.Following encapsulation in dialysis membranes, the specimens were transferred into a conical flask containing phosphate buffer (pH 7.4), maintained at 37 °C, and subjected to constant rotation at 100 rpm. One milliliter sample was removed from the outer solution and replaced with brand-new PBS at pH 6.8 at predefined intervals. These aliquots were filteredand analyzed using the HPLC method at 270 nm to measure drug release. Three duplicates of the experiment were carried out[22].

Stability studies

The optimized formulation's stability was evaluated by storing it at three temperatures (4°C, 25°C, and 40°C) at 75% relative humidity. Regular intervals were set to measure particle size, PdI,ZP, and EE changes in the samples[23]

Pharmacokinetic studies(PKs)

The Nutrition National Institute (NIN), situated in Telangana, India, provided the male Wistar rats used in the study, which had an approximate weight of 200 ± 20 g and an age of 4-5 weeks. The animal study followed the guidelines as per the Care and Use of Laboratory Animals. The Institutional Animal Ethics Committee (IAEC)

officially sanctioned the protocols designated by the assigned protocol number (1447/PO/Re/S/11/CPCSEA-86/A). Animals were exposed to natural light/dark settings for one week, acclimating to a relative humidity of 40–60% and a temperature of 20 ºC ± 2 ºC. After that, they were randomly divided into two groups of six animals. The optimized drug-loaded NBs (40 mg/kg BW)and the pure drug (dispersed in 0.5% w/v carboxymethylcellulose) were administeredby oral route.The animal blood was obtained from the retroorbital plexus (300 µL) and then transferred into sterile test tubes with EDTA at specific intervals (0.25, 0.5, 1, 2, 4, 6, 12, 24,48 and 72 h).Blood samples were centrifuged at 7500 rpm for ten minutes using an Eppendorf centrifuge. The resulting plasma was further analyzed using high-performance liquid chromatography(HPLC)[12]. The drug was recovered from plasma samples *via* the protein precipitation method. The drug was successfully extracted from plasma by adding acetonitrile (250 µL) to rat plasma (50 µL) and vortexed. The supernatant was centrifuged for 12 minutes at 8000 rpm and then analyzed using Chromatography at a λmax of270 nm. Non-compartmental analysisWinNonlin (version 3.1; Pharsight et al., USA) was employed to calculate the Cmax (maximum plasma concentration, (AUC0-72) area under plasma concentration *vs*time curve from 0 to 72 h, Tmax (time to reach the maximum plasma concentration, Kel (elimination rate constant, t1/2 (half-life). All the data were expressed as mean ± SD.

3. RESULTS

Enzalutamide nanobubbles (ENZ-NBs) formulation development and **optimization**

The study aimed to formulate enzalutamide nanobubbles by integrating ultrasound technology with solvent evaporation. The drug had been mixed with PLGA that had been dissolved in DCM, sonicated, and added to a cooled 1.9% w/v PVA solution. After that, a 3-minute sonication at 30 W and high-speed homogenization were done. Isopropanol solution(2.5% v/v) was used to extract dichloromethane. For extracting, isopropanol was mixed under stirring for five hours. The word "nanobubbles" was chosen over "nanodroplets" because perfluoropentane is a fluid substance at normal temperature. Acoustic droplet vaporization, a liquid-to-vapor phase change brought on by ultrasound, converted nanodroplets into nanobubbles, enhancing their echogenic qualities in ultrasonography photographs24. The term "ultrasound" refers to pressure waves with compressional and rarefactional fluctuations at frequencies ≥20 kHz, leading to effects such as cavitation for bubble size reduction and sonoporation, which helps to uptake the reduced bubbles25.Electron microscopy helped for the direct visualization of nanobubbles and for assessing the integrity of nanobubbles and for its gas composition. By combining ultrasound with nanobubbles, drug localization can be achieved while mitigating off-target side effects26.Hydrophobic interactions play a crucial role in bonding PLGA with the drug while forming nanobubbles, while polyvinyl alcohol (PVA) acts as a stabilizing agent. PVA creates a protective coating around the nanobubbles to uphold their stability.Due to its biocompatibility and biodegradability properties, PLGA is highly recommended in various medical applications, including sutures, bone implants, and sustained drug release systems.Quality by Design (QbD) emphasizes precisely monitoring critical quality attributes (CQAs) to achieve and maintain QTPP.NBs aim to enhance drug stability, bioavailability, and targeted delivery, addressing solubility and short half-life issues. The current study selected PS, PdI, ZP, and EE as CQAs (Table 2). Multiple linear regression analysis (2FI) constructed polynomial models (quadratic, two-factor, and linear). The model selection used R2, predicted R2, adjusted R2, and coefficient of variance (C.V). ANOVA assessed variable impact on responses.

Table 2:BBD and the experimental data

Factor 1	**Factor 2**	**Factor 3**	**Response 1**	**Response 2**	**Response 3**	**Response 4**
A: Stabilizer concentration	B:Homogenization Speed	C:Homogenization time	PS (Y1)	PdI (Y2)	ZP (Y3)	EE (Y4)
%	rpm	mins	nm		mV	%
1.5	15000	5	210.	0.35	20.1	50.8

			81	5	1	2
1	12500	5	282.3	0.429	17.03	68.27
2	12500	15	226.2	0.318	27.02	76.79
2	12500	5	236.84	0.432	27.98	63.86
1	12500	15	280.6	0.468	15.8	73.68
1.5	10000	5	260.36	0.381	21.02	73.6
2	10000	10	189	0.262	28.92	63.29
1.5	12500	10	172.8	0.251	24.56	65.32
2	15000	10	178.44	0.289	30.4	62.51
1.5	12500	10	199.08	0.223	26.3	63.21
1.5	12500	10	197.4	0.218	26.44	62.96
1.5	12500	10	196.2	0.236	26.99	63.29
1.5	15000	15	228.22	0.364	19.94	73.28
1	10000	10	244.2	0.342	19.56	74.19
1.5	12500	10	199.6	0.223	26.22	63.48
1.5	10000	15	186.9	0.271	19.85	70.77
1	15000	10	241.8	0.369	18.32	54.21

PS

The small size of NBs results in a significantly higher surface area-to-volume ratio, enhancing their stability, penetrability, and reactivity in targeted drug delivery[19]. After 17 trials, particle size ranges from 172.8 to 282.3 nm. The model's F value of 17.28, with a 0.01 percent chance of being noise, confirmed its 'quadratic' nature and lack of fit is insignificant. ANOVA found variables with p-values below 0.0500 that significantly impacted the response. The “lack of fit F-Value” (0.73) implies that any lack of fit is not statistically considerable. There is 58.73 % chance that a “Lack of Fit F-value” of this extent would occur due to random noise, underscoring the model’s reliability. The contour plots (CP)and 3D response surface plots (RSP) are illustrating variable influences on particle size (PS) are depicted in Figure 1. The R^2 corrected R^2 and anticipated R^2(0.9569, 0.9016, and 0.7119) respectively, showing a model precision of 13.23, surpassing the required value of 4. Stabilizer concentration (A) with a high negative coefficient is the most influential factor affecting particle size, demonstrating that alterations in this factor result in a corresponding change in particle size. Homogenization speed and time, denoted by variable B and C, also plays a role in particle size, although to a lesser extent than stabilizer concentration.The interaction terms (AB, AC, and BC) suggest the combined effects of these variables and had a significant impact on particle size. While the positive coefficients for quadratic terms like A^2 AB^2, and C^2 suggest that the squared values of A, AB, and C have a nonlinear relationship with particle size, potentially leading to changes in particle size that are not directly proportional to changes in the variables.Modelterms (A, BC, A^2, and C^2) had p-values < 0.0500, signifying a significant effect. The resulting

International Journal of Environmental Sciences
ISSN: 2229-7359
Vol. 11 No. 2, 2025
https://www.theaspd.com/ijes.php

regression equation is:

$$Particle\ size = 193.02 - 27.30\,A - 2.65B - 8.55C - 2.04AB - 2.24AC + 22.72BC + 27.63A^2 - 7.28AB^2 + 35.84C^2$$

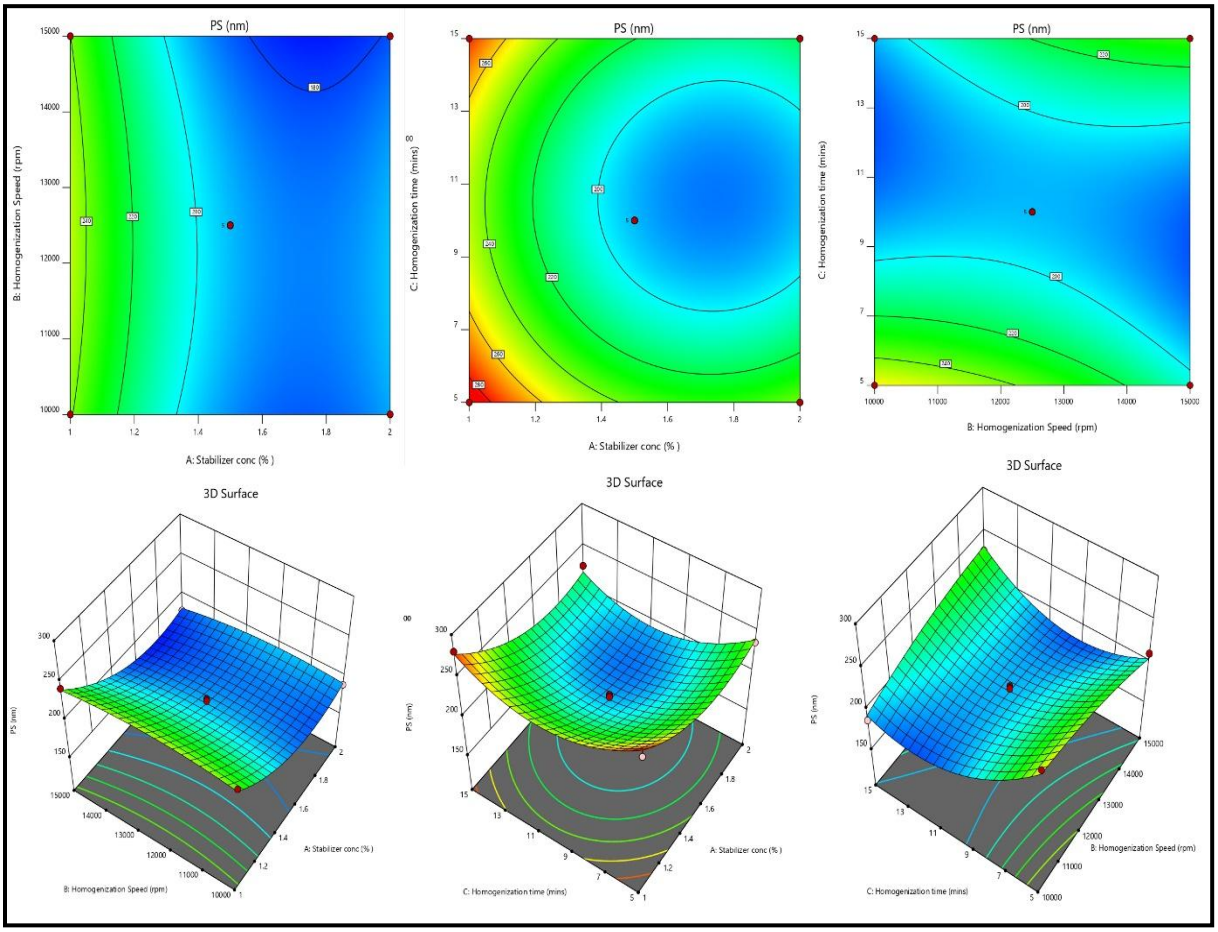

Figure 1: Contour plots (CP)and Response surface plots(RSP) illustrating variable effects on particle size (PS).

PdI

The polydispersity index (PdI) is a dimensionless metric that quantifies the broadness of the particle size distribution[27]. Typically, it falls between 0 and 1. Formulations exhibited PdIs from 0.218 to 0.468, with a model F value of 94.76, indicating the significance of the proposed "quadratic" model and an insignificant lack of fit (F-value 0.24). There is 86.80 % chance that a "Lack of Fit F-value" of this magnitude would arise due to random noise, underscoring the model's reliability. Regression coefficients (R^2, adjusted R^2, and anticipated R^2) were 0.9919, 0.9814, and 0.9697, correspondingly, showing model's usefulness with precision exceeding the necessary value (28.0180). Model terms (A, B, C, AC, BC,A^2, and C^2) had p-values < 0.050, signifying a substantial impact. The resulting regression equation is:

$$PDI = 0.2302 - 0.0384A + 0.0151B - 0.0220C + 0.00AB + 0.0383AC + 0.0297BC + 0.0771A^2 + 0.0081B^2 + 0.1044C^2$$

Positive coefficients signify a rise in the associated variable(s), which increases PdI, while negative coefficients indicate a decline, which reduces PdI. An increase in variable A (stabilizer concentration led to a decrease in PdI whereas higher values of B and C (homogenization speed and homogenization time lead to higher PdI. The interaction terms AC (0.0383) and BC (0.0297) both have positive coefficients, suggesting that the combined effect of variables A and C, as well as B and C, tends to increase the PDI. All quadratic terms have positive coefficients, indicating that increases in the squared values of variables A, B, and C lead to increases in the Polydispersity Index.The graphical image of response surface and contour plots illustrating variable effects on polydispersity index (PdI) is shown in Figure 2.

International Journal of Environmental Sciences
ISSN: 2229-7359
Vol. 11 No. 2, 2025
https://www.theaspd.com/ijes.php

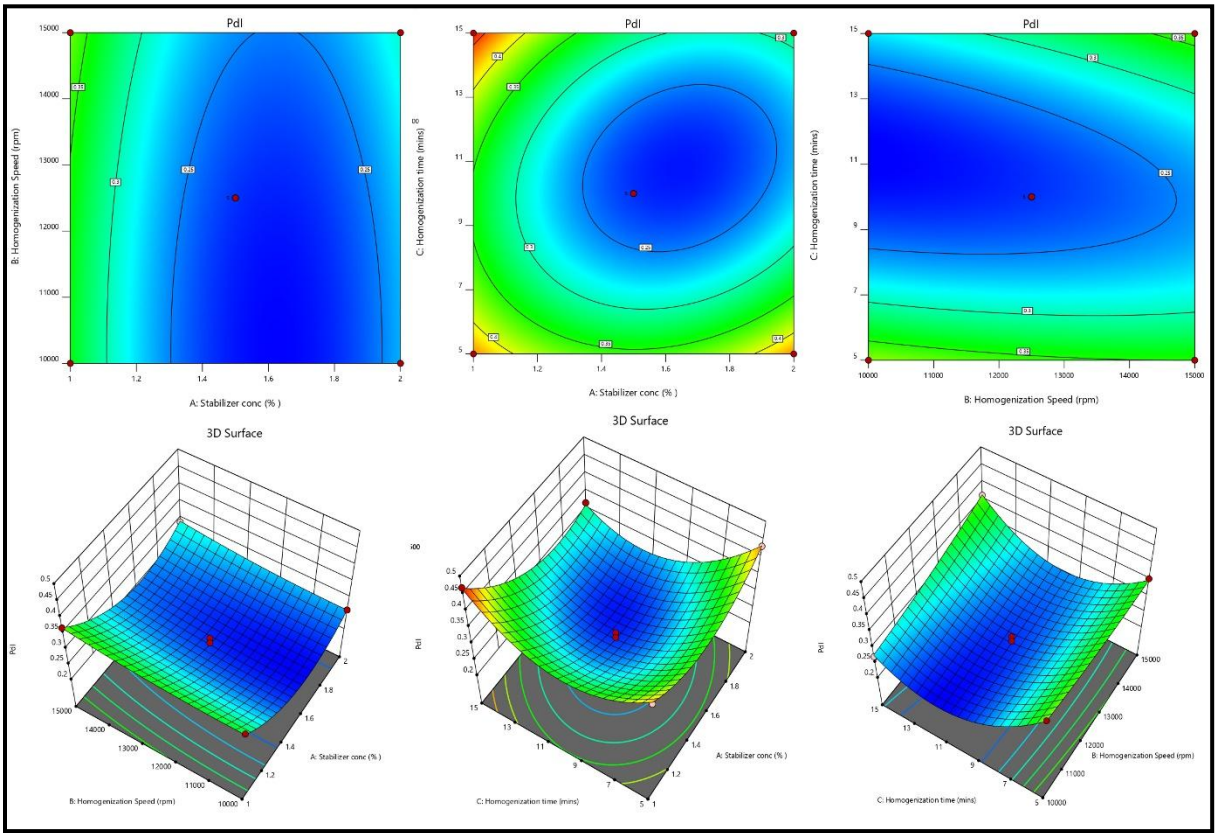

Figure 2: Graphical depiction of contour plotsand response surface plots illustrating variable effects on polydispersity index (PdI)

Zeta potential

It is influenced by surface charges, shows an important role in the stability of nanoparticles suspension and the initial interaction of nanoparticles with cell membrane, making it crucial for effective drug delivery[15]. In our study the zeta potential of nanobubbles ranged from 30.40 mV to 15.8 mV. The quadratic model for zeta potential demonstrates notable statistical significance, illustrated by the substantial F-value of 70.60. Regression coefficients (R^2, adjusted R^2, and anticipated R^2) were 0.9891, 0.9751, and 0.9701, respectively. The predicted R^2 aligns closely with the adequate R^2, differing by 0.2. The model, evidenced by adequate precision (signal-to-noise ratio) of 25.99, surpassing the necessary value of 4, proved helpful in exploring the design space.The variables (A, B^2, and C^2) substantially affected zeta potential, with a P value below 0.0500. The "lack of fit F-value" (0.12) indicates that any lack of fit is not statistically significant. There is a 94.43 % chance that a "Lack of Fit F-value" of this magnitude would arise due to random noise, underscoring the model's reliability. A non-significant Lack of fit is good, and we want the model to be fit.Consequently, these terms are deemed necessary, and the resulting regression equation is as follows:

$$Zeta\ Potential(ZP) = +26.10 + 5.45A \quad - 0.02725B - 0.4412C + 0.6800\text{AB} + 0.0675AC + 0.2500BC - 0.0373A^2 \ - 1.76B^2 \ - 4.11C^2$$

Positive coefficients indicate a positive connection, which implies that a rise in the associated variable or variables causes an increase in ZP.The negative coefficients imply a negative correlation, which shows that a decline in the related variable or variables causes a reduction in ZP. The CP andRSP demonstrating the consequence of variables on ZP are shown in Figure3.

International Journal of Environmental Sciences
ISSN: 2229-7359
Vol. 11 No. 2, 2025
https://www.theaspd.com/ijes.php

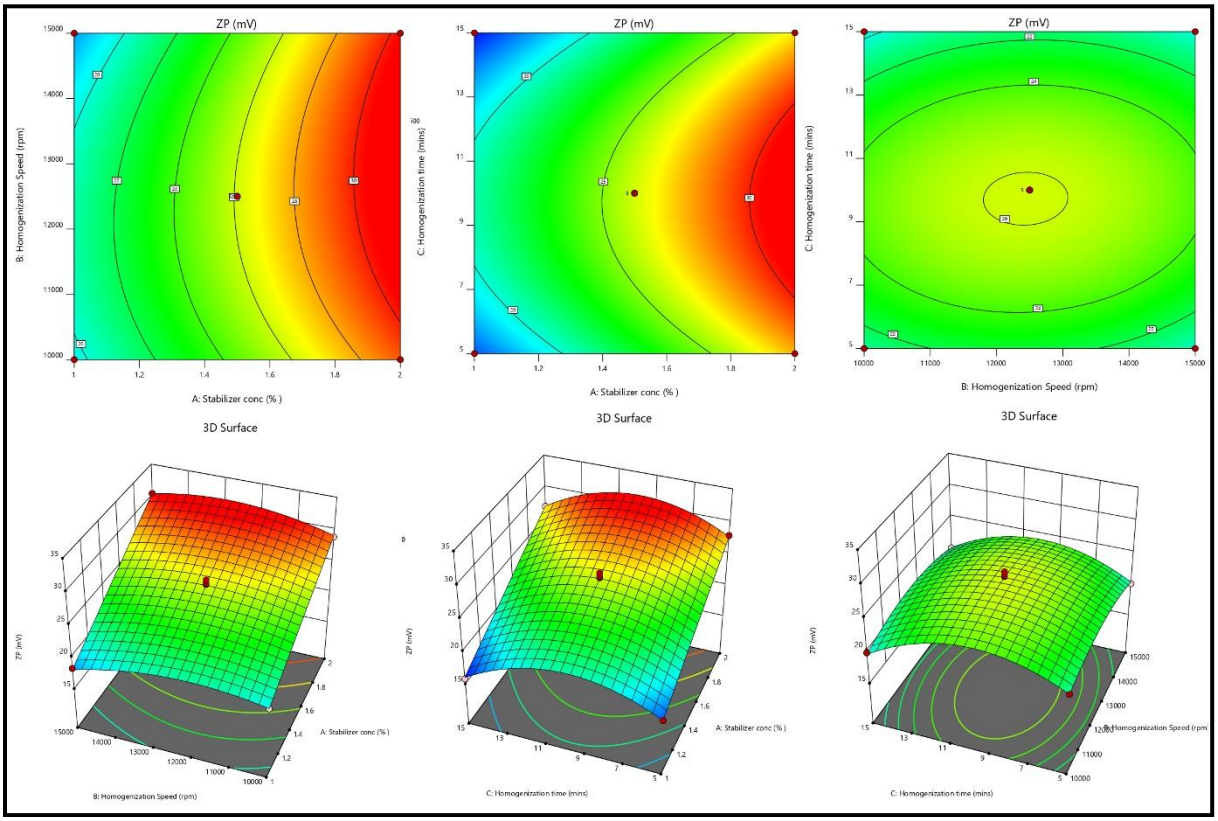

Figure 3: graphical depiction of contour plots and response surface plots showing the variable effects on Zeta potential(ZP)

Entrapment efficiency (EE)

Impact on EE ranges from 50.82 to 76.79 percent. The NB with high entrapment is always desirable to reduce the dose of the drug. The model's F value 153.34, with a 0.01% chance likely due to noise, indicates significance and negligible fit error for the suggested "quadratic" model. The lack of fit's F-value(0.17) is not statistically significant based on pure error, with a 91.43% probability of being noise. ANOVA identified significant factors (p-value < 0.1000), leading to the removal of non-significant variables. Figure 4 illustrates the CP and 3D SP, which showcase the influence of selected variables on EE. The regression coefficients, R^2, adjusted R^2, and anticipated R^2, were 0.9950, 0.9885, and 0.9841, respectively. The predicted R^2 aligns closely with the adequate R^2, differing by 0.2. The model, evidenced by adequate precision (signal-to-noise ratio) of 44.253, surpassing the necessary value of 4, proved helpful in exploring the design space. The CP andRSP demonstrating the consequence of variables on ZP are shown in Figure4. An elevation in factors A and B (stabilizer concentration) typically results in decreased entrapment efficiency, whereas elevations in factors C(homogenization speed and duration) tend to increase efficiency. In contrast, the interaction terms and quadratic terms increased the EE. By comprehending the impact of these factors on entrapment, researchers can fine-tune formulations to attain desired levels of efficiency, thereby guaranteeing the effective delivery of substances in pharmaceutical or other applications.Modelterms (B, C, AB, AC, BC, A^2, B^2, and C^2) had p-values < 0.0500, signifying a significant effect. The resulting regression equation is:

$$Entrapment\ efficiency\ (EE) = +63.65 - 0.4875A - 5.13B + 4.75C + 4.48AB + 1.88AC + 6.32BC + 1.72A^2 - 1.82B^2 + 5.28C^2$$

International Journal of Environmental Sciences
ISSN: 2229-7359
Vol. 11 No. 2, 2025
https://www.theaspd.com/ijes.php

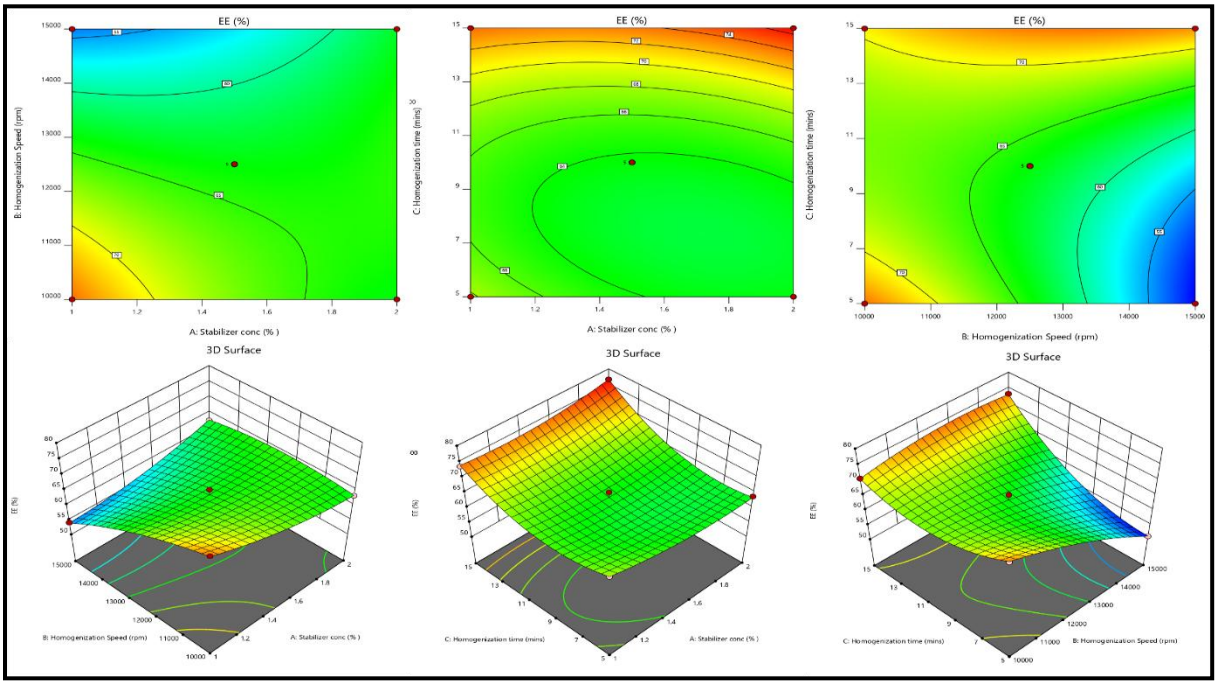

Figure 4: Graphical representation of response surface plots (RSP) and contour plots (CP) demonstrating its consequence of variables on EE.

Exploration for optimized preparation

The Derringers desirability method was employed to enhance the factors that impact response parameters. This method entails converting responses into a desirability scale and combining them into a geometric mean function using thorough searches, ultimately resulting in a universal desirability value.The optimum configuration (Fopt solution) with the drug is 40 mg, stabilizer (PVA) at 1.9 %w/v with a homogenization speed at 12200 and homogenization duration of 12, resulting in a D value of 0.825. Further graphical customization was made possible by restricting the level of critical quality attributes (CQAs), specifically low PS and PdI, with a rise in ZP andEE.Figure 5 presents the design space and overlay plot. Throughout the validation process, three checkpoints were employed to confirm the model's strength and formulation. The anticipated average size standards were 190.7 nm with a PdI of 0.244, ZP of 29.68, and EE of 67.77, whereas the actual average measurements were 193.5 ± 2.8 nm, PdI of 0.261 ± 0.016, ZP of 31.4 ± 1.17 and EE of 65.12 ± 2.54.

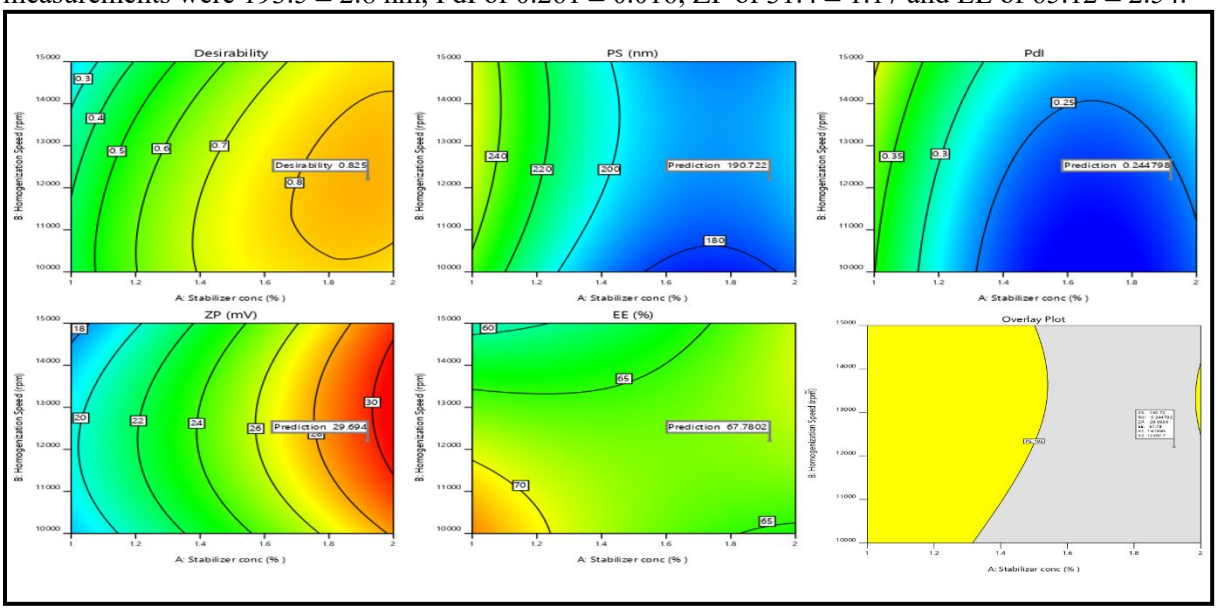

Figure 5: *Graphical illustration of desirability and Overlay plot (yellow area denotes the feasible region)*

International Journal of Environmental Sciences
ISSN: 2229-7359
Vol. 11 No. 2, 2025
https://www.theaspd.com/ijes.php

CHARACTERIZATION AND EVALUATION OF NANOBUBBLES (NBS):

PS, PdI, zeta potential (ZP), and entrapment efficiency (EE) measurements.

Particle sizes and uniformity in the formulation remained consistent, with PS ranging from 193.5 ± 2.8 nm and PdI from 0.261 ± 0.016.A polydispersity value below 0.3 indicates homogeneity. The optimized formulation's zeta potential, indicative of colloidal particle surface properties, was 31.4 ± 1.17 mV, with an EE of 65.12 ± 2.54.The particle size and ZP of the optimized nanobubbles are shown in Figure 6. Nanobubble stability heavily relies on elevated zeta potentials, which play a crucial role in maintaining electrostatic repulsion among particles, thus preventing their aggregation. This stability is of utmost importance as it ensures the integrity of nanobubbles during storage and administration, ultimately enhancing their performance in drug delivery and medical imaging applications.

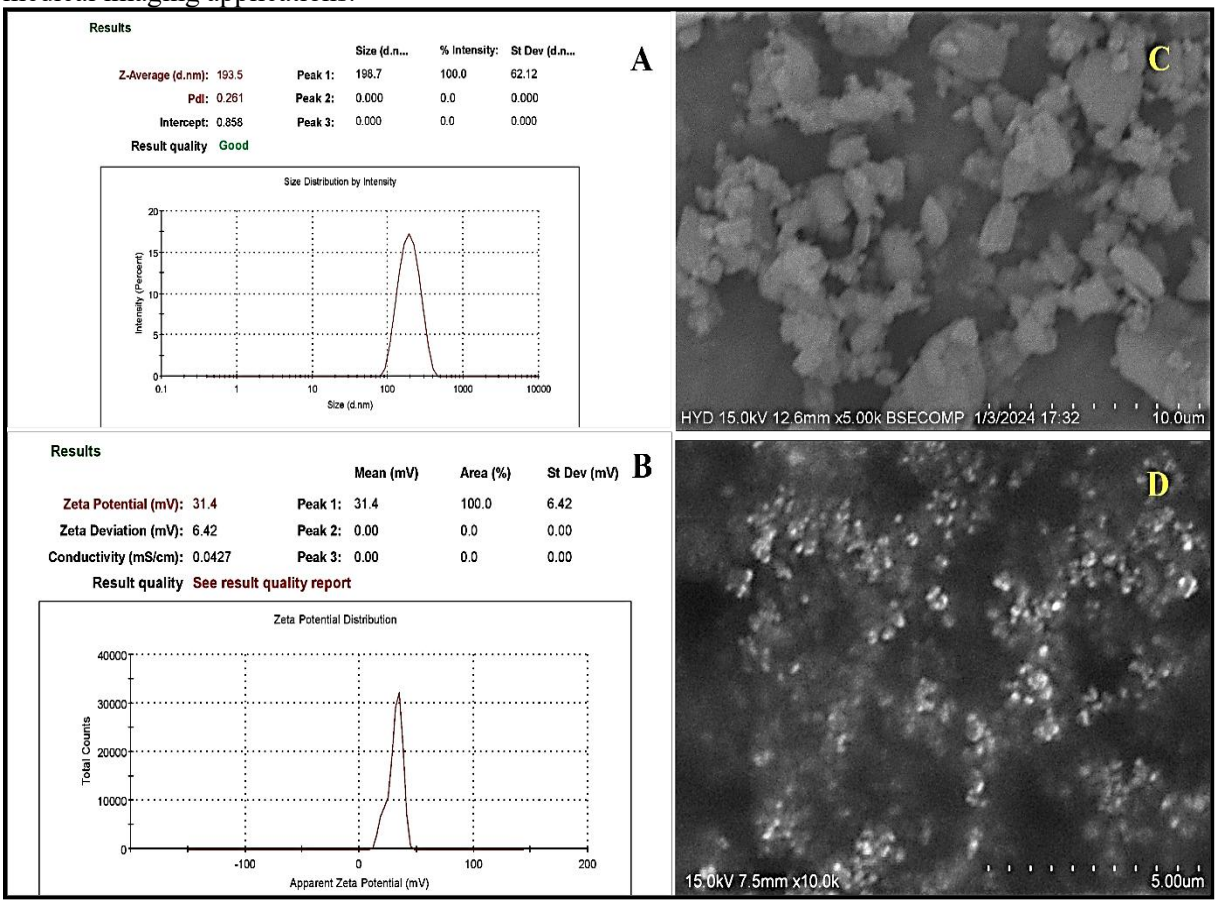

Figure 6: Malvern image of A) Particle size &PdI; B) ZP; C) SEM image of pure drug; D) ENZ-PLGA Nanobubbles (NBs)

Fourier Transform Infrared Spectroscopy study (FTIR)

The interaction between the drug and the polymer used in nanobubble formulation was investigated through FTIR analysis(Figure 7). The IR spectra of the drug confirming the purity of ENZ drug and PLGA peaks are mentioned in Supplementary Table 1.The FTIR spectra of optimized formulation (NBs) show the drug's peak characteristics, showing minor changes that hint at potential hydrogen bonding linking the drug -OH groups with PLGA's C=O groups. The ENZ encapsulated in the polymer matrix implies no chemical interaction[13]

International Journal of Environmental Sciences
ISSN: 2229-7359
Vol. 11 No. 2, 2025
https://www.theaspd.com/ijes.php

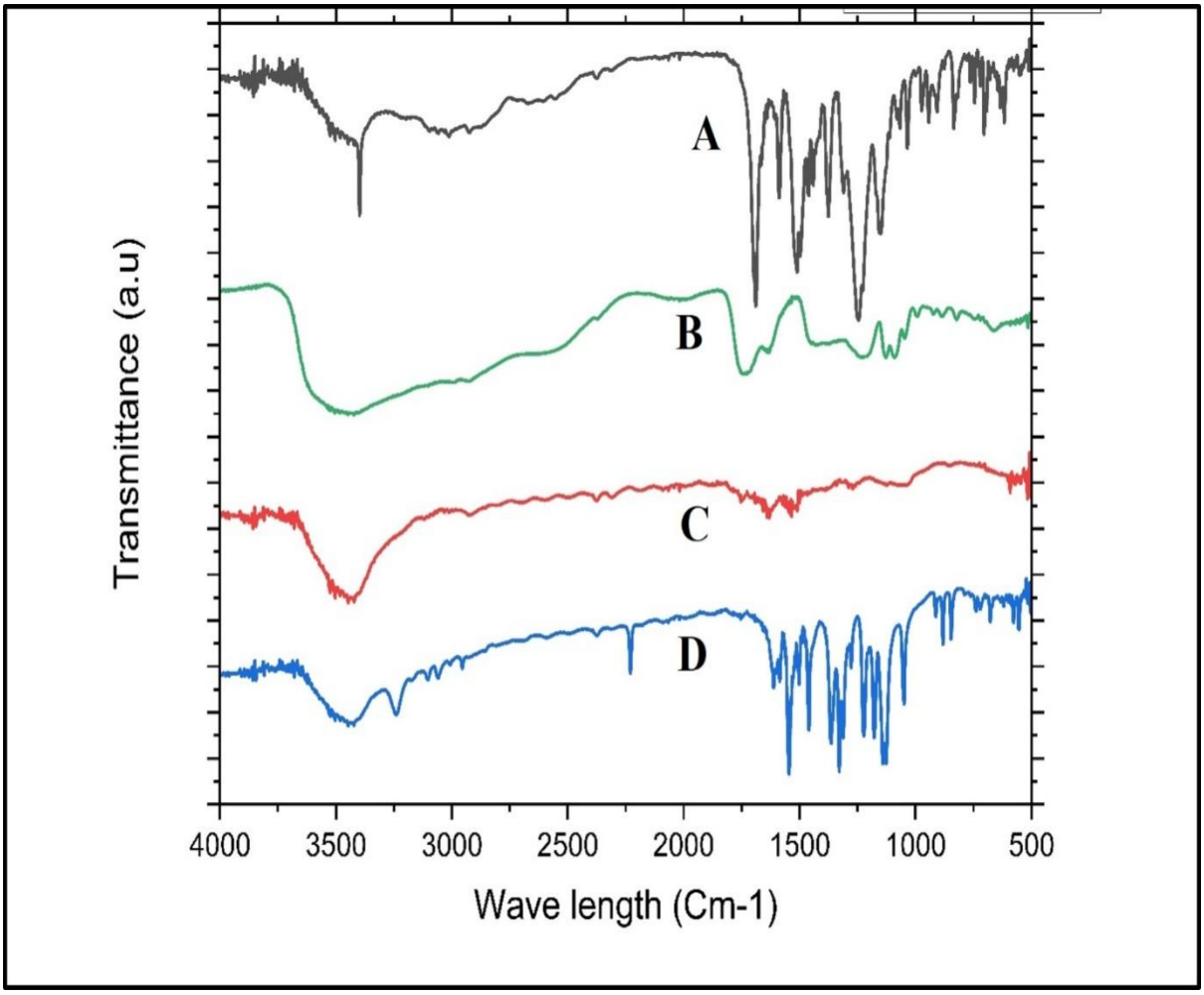

Figure 7: A) Overlay of FTIR analysis A: PD (black line- pure drug; B: PLGA (green line); C: PM (red line- Physical mixture; D: drug loaded NBs (Blue line- Nanobubble (NS).

DSC and XRD

DSC assessment was accomplished to evaluate the thermal characteristics of the drug, PLGA, and the nanobubbles pre and post-storage for a duration of 3 months(Figure 8). The pure drug exhibited a clear endothermic peak at 145.26°C, signifying its melting point, and a broad peak at 194.52°C, indicating its crystalline characteristics[13].

The thermograph of PLGA exhibited peaks at 61.8°C and 163.17°C. In the thermographs of the nanobubbles, two peaks emerged at 145. 63°C and 187.78°Cindicate a minor shift in the melting point of the drug and its confinement within the polymeric structure due to weak intermolecular interactions between the drug and the polymer.

The XRD patterns are depicted in Figure 6 B. The drug has displayed firm diffraction peaks (2 θ scattered angles of 8.5, 12.2, 13.3, 14.1, 17.3, 18.8, 19, 19.6, 20, 21.6, 22.4, 23.2, 24.2, 24.6, 26, 26.8, and 27.3°) confirming its crystalline nature. Previous studies have also reported similar diffraction peaks for the drug under study. However, in the nanobubbles, the characteristic diffraction peaks of ENZ vanished, suggesting the pure drug may have formed a solid-state complex at a molecular level in the nanobubbles.

International Journal of Environmental Sciences
ISSN: 2229-7359
Vol. 11 No. 2, 2025
https://www.theaspd.com/ijes.php

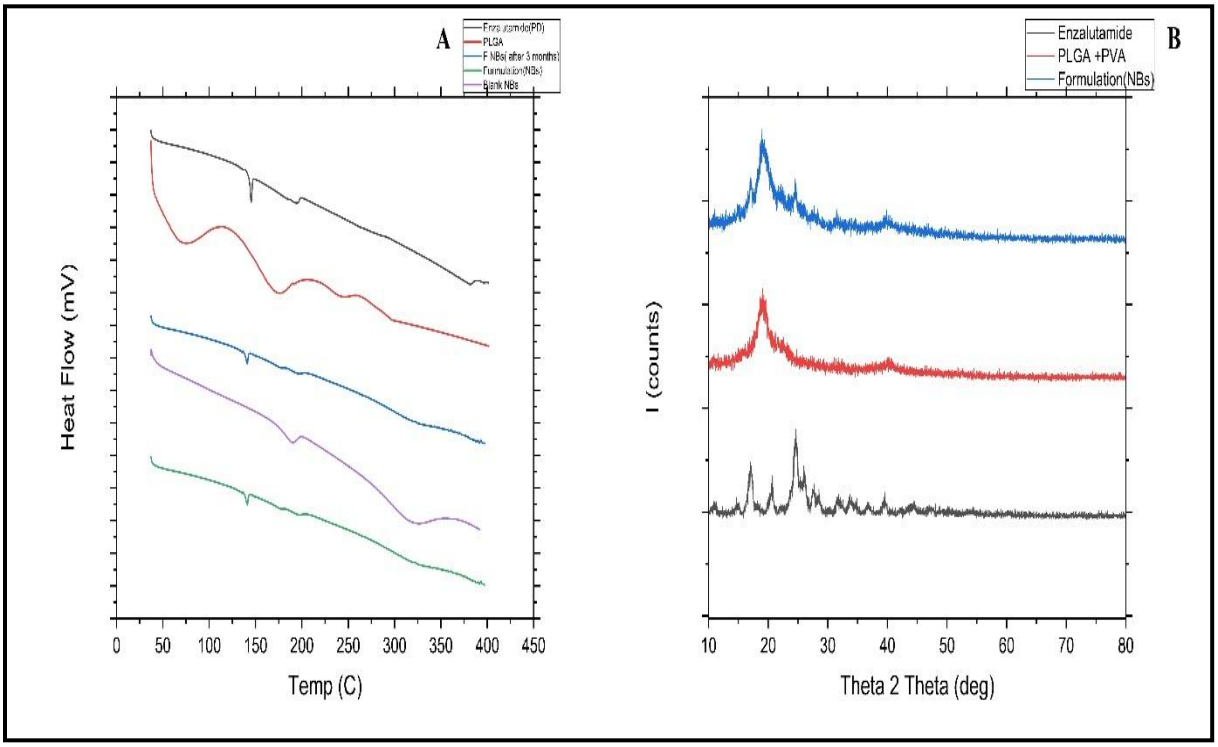

Figure 8:A) Overlay of DSC thermograms of i) Enzalutamide PD (black line);ii) PLGA (red line);iii) Formulation of NBsstored for 3 months (blue line); iv) Formulation (optimized NBs green line); v) Blank NBs (purple line) B) Overlay of XRD of i) Enzalutamide - PD(black line); ii) PM(PLGA+ PVA + Drug- red line); iii) Formulation-NBs(blue line).

Drug release (DR):

Figure 9 depicts dissolution profiles of plain drug and drug-loaded nanobubbles without and with acoustic assistance. Drug release from nanobubbles was significantly higher than a simple drug suspension. Notably, ultrasound assistance increased drug release. The cumulative drug release (CDR) at 8 hour was 16.03 ± 3.32%, 44.64 ± 4.61%, and 78.84 ± 4.04 % for plain drug, nanobubbles without acoustic, and with acoustic, respectively. By 48 h, over 98.24 ± 8.18% was released from nanobubbles with acoustic assistance and 65.79 ± 7.29% without acoustic, but in the case of the pure drug, only 32.02 ± 5.23% of the drug was released. Drug release occurred due to collapse cavitation induced by acoustic waves, disrupting nanobubble structures and enabling rapid medication release. Acoustic waves, with meticulous control and non-invasive nature, offer accurate drug delivery and targeting abilities. These findings confirm that ultrasound assistance plays a pivotal role in enhancing drug release from the nanobubbles potentially through the cavitation effect induced by ultrasound. Ultrasound stability studies indicated the transformation of the gas core from nanodroplets to bubbles, known as acoustic droplet generation. Under the influence of ultrasound, the oscillation of bubbles can trigger the shell to open, thereby aiding in the release of drugs. The study aligned with previous findings on nanobubble stability under varying temperature conditions. The acoustic streaming flow generated by bubble oscillation regulates the movement of detached materials, which is influenced by both the radial excursion and the duration of the ultrasound pulse[28].

Regulated and non-invasive acoustic waves are ideal for precise drug administration and targeting.

International Journal of Environmental Sciences
ISSN: 2229-7359
Vol. 11 No. 2, 2025
https://www.theaspd.com/ijes.php

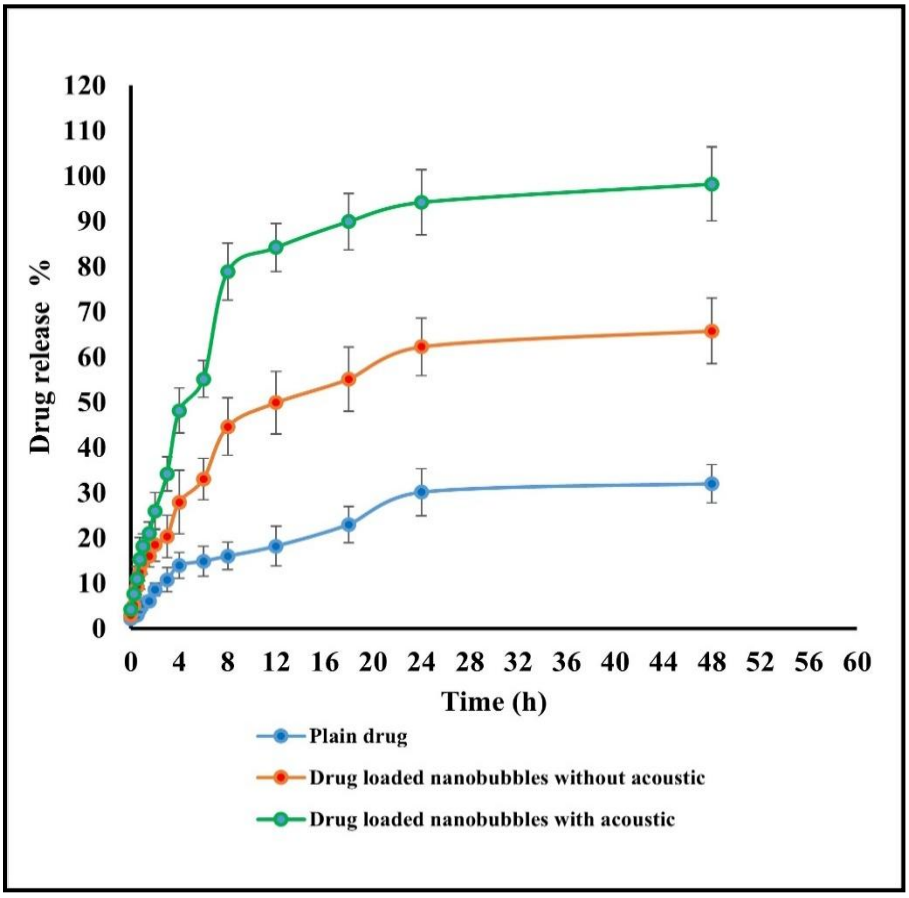

Figure.9*In-vitro*drug release of plain drug, drug loaded nanobubbles with and without ultrasound aid.

Stability studies

ENZ-loaded nanobubbles (NBs) underwent stability assessments atvarious storage conditions (4 °C, 25 °C, and 40 °C) for 0, 1 month, two months, and three months (Table 4). At 4 °C and 25 °C, minimal changes in drug content indicated robustness, with encapsulation efficiency (EE) showing slight variation, suggesting protection against degradation. However, a notable reduction in EE occurred at elevated temperatures,where EE was reduced to 62.41± 3.90 % from 65.12 ± 2.54, indicating structural disruption. Throughout the experiment, the PS of the formulation is less than 200 nm, and the zeta potential is around 29 ± 2.29mV, highlighting the stability and uniformity of ENZ nanobubbles. Storage in a polyethylene (PE) pouch led to a faster drop in number concentration compared to a glass bottle.Hydrogen bonding interactions were emphasized as critical factors in forming bulk nanobubbles and their exceptional long-lasting stability[28]

Pharmacokinetic studies

Figure 10displays the plasma concentration-time curve after drug administration in 0.25% w/v sodium carboxymethylcellulose solution and the optimized nanobubbles orally. Pharmacokinetic data in Table 3 reveal that the formulation exhibited significantly higher Tmax, Cmax (**$p < 0.001$), AUC0-24 (**$p < 0.001$), and AUC0-∞ (**$p < 0.001$) values compared to the pure drug suspension at the prescribed dose. The bioanalytical chromatogram indicated drug retention time at 12.7 min and internal standard (Nilutamide) at 9.5 min (Figure 11).

The optimized formulation reached a maximum level (Cmax) of 6.84 times higher, while the area under the curve (AUC_{0-t}) was 5.874times higher than the free drug.In-vivo studies revealed a progressive drug release from the nanobubble preparation with extended Tmax.Comparing the data to the free drug, oral bioavailability has significantly improved. This finding suggests a notable improvement in oral bioavailability compared to the free drug. The enhanced bioavailability can be attributed to the increased drug circulation at the nanoscale and the improved penetration facilitated by the polymeric carrier system.

International Journal of Environmental Sciences
ISSN: 2229-7359
Vol. 11 No. 2, 2025
https://www.theaspd.com/ijes.php

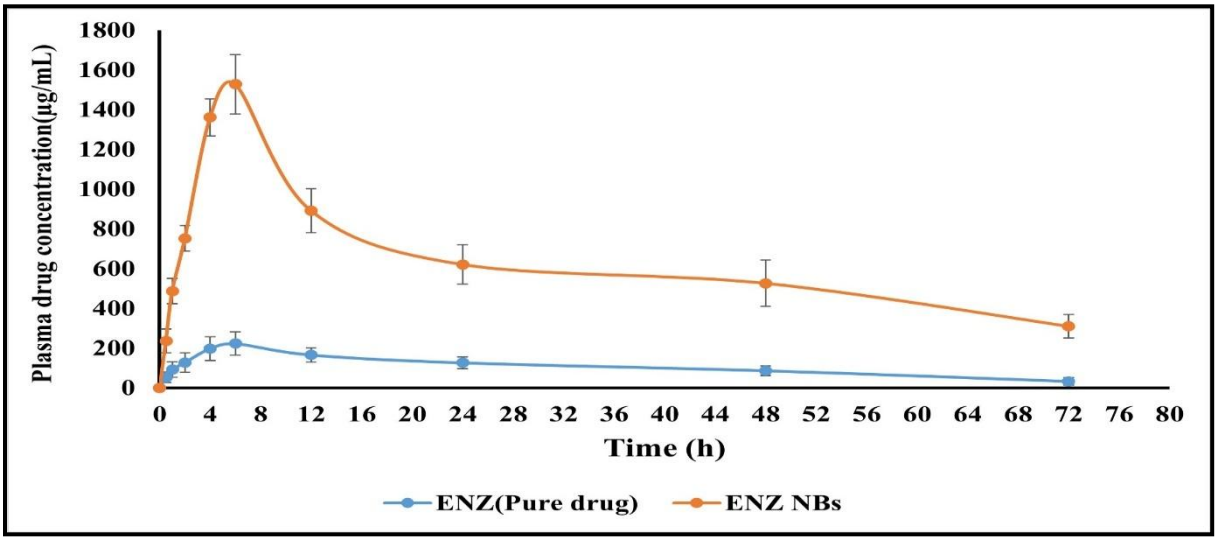

Figure10 :*In vivo* pharmacokinetic studies

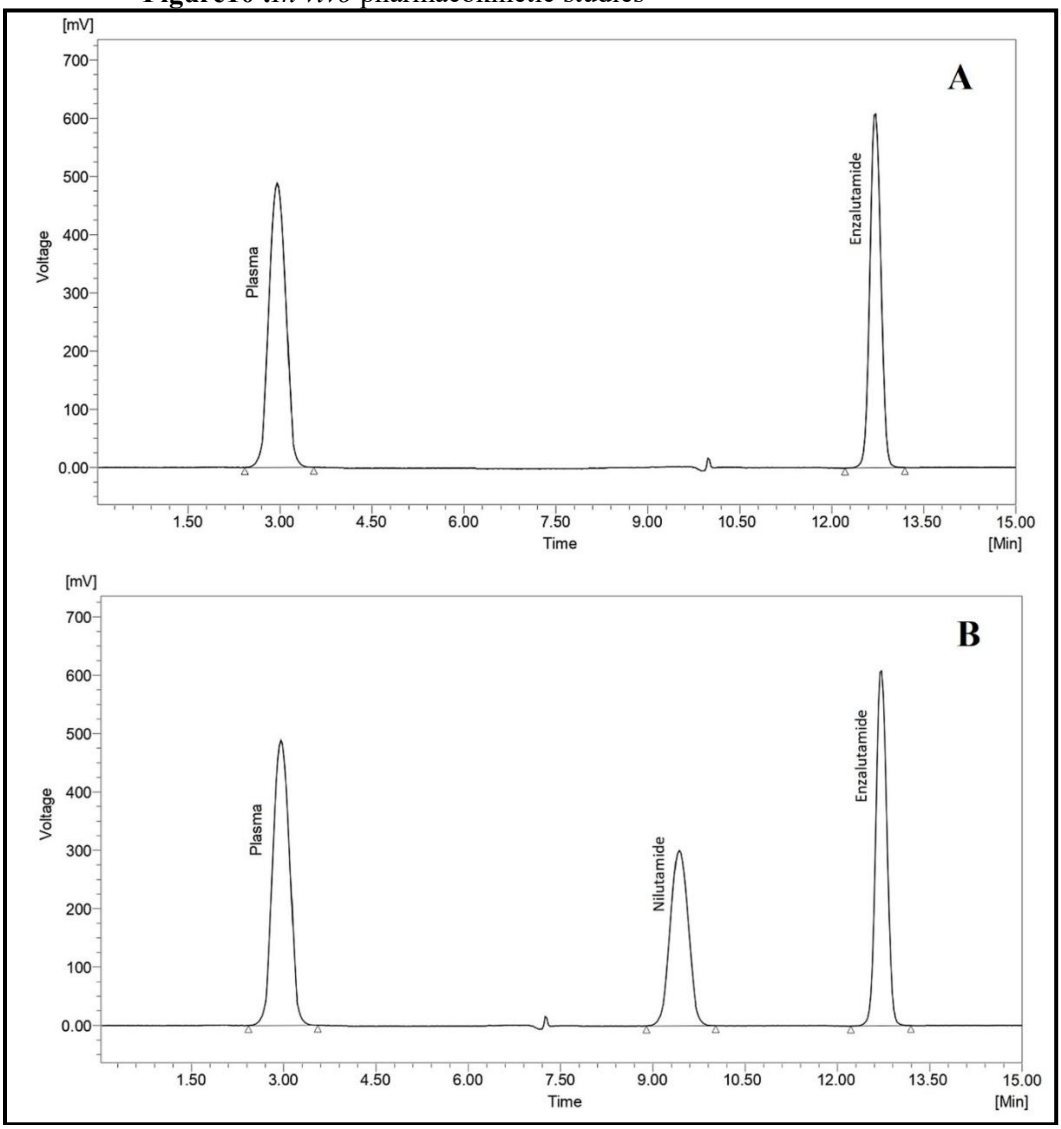

Figure 11: The bioanalytical chromatogram drug in plasma (A) ; Drug and internal standard in plasma indicated drug retention time at 12.7 min and internal standard (Nilutamide) at 9.5 min.

Table 3: Pharmacokinetic parameters

Pharmacokinetic parameters	Pure drug	Drug loaded NBs
C_{max} (ng/mL)	223.2± 58.04	1528.06± 148.66
T_{max} (h)	6	6
Half-life (h)	26.09± 2.58	43.07± 3.13
AUC $_{0-t}$ (ng. h/mL)	7833.88± 263.16	46022.12± 586.82
AUC $_{0-inf}$ (ng. h/mL)	9082.47± 420.17	65297.31± 546.20
Ke (h^{-1})	0.0265	0.0160
MRT(h)	38.036± 5.44	59.348±6.20

4. DISCUSSION

In this study, ENZ-loaded PLGA nanobubbles were formulated using the solvent evaporation method, with optimization conducted through the Box-Behnken design (BBD). NBs are emerging as a formulation strategy because of their targeting ability. The process in which nanodroplets in perfluoropentane transition from liquid to vapor upon exposure to ultrasound waves is called acoustic droplet vaporization24.Perfluoropentane undergoes a phase transition that turns nanodroplets into nanobubbles with high ultrasonic (US) wave reflectivity. The echogenic qualities of perfluoro pentane make them visible in ultrasonography images23. The NBs were developed using PLGA polymer containing unbound carboxylic end chains using perfluoro pentane for the inner core and PLGA as the outer shell25.The term "ultrasound" describes mechanical vibrations or pressure waves that exhibit compressional and rarefactional pressure fluctuations and have frequencies equivalent to or higher than the human hearing threshold (20 kHz).Ultrasound effects primarily involve two mechanisms: cavitation and sonoporation. The cavitation effect plays a crucial role in reducing the size of bubbles, whereas the sonoporation effect facilitates the uptake of these reduced bubbles15.Combining ultrasound with nanobubbles helps in drug localization while overcoming the off-target adverse effects. The nanobubbles using PLGA have garnered attention for targeted drug delivery because of their unique physical and surface properties. PLGA is highly recommended in various medical applications, including sutures, bone implants, and sustained drug release systems, due to its biocompatibility and biodegradability properties29.The quadratic model suggested by the design was applied to PS, PdI, ZP, and EE. Positive coefficients in the model indicated a positive connection, signifying that an increase in associated variables led to higher drug entrapment. Stabilizer concentration has affected particle size, PdI, and ZP. However, when it came to EE, a high stabilizer concentration led to a decrease in drug entrapment. PVA, as a stabilizer, has the potential to impede drug entrapment in nanobubbles due to its competition for surface adsorption and the subsequent increase in solution viscosity. Moreover, PVA may hinder drug diffusion into nanobubbles during the formation process. Furthermore, its destabilizing effects can result in premature rupture or aggregation, ultimately diminishing the efficiency of drug entrapment30.FTIR studies confirmed compatibility between drug and excipients. DSC and XRD studies revealed no distinct drug peak in the formulation, indicating the absence of crystalline drug material13. SEM analysis displayed homogeneous, smooth, spherical-shaped nanobubbles. Drug release occurred due to collapse cavitation induced by acoustic waves, disrupting nanobubble structures and enabling rapid medication release. Ultrasound stability studies indicated the transformation of the gas core from nanodroplets to bubbles, known as acoustic droplet generation31. The study aligned with previous findings on nanobubble stability under varying temperature conditions. The temperature-dependent behavior observed in particle size, ZP, and entrapment emphasized understanding nanobubble characteristics in diverse environmental conditions for practical drug delivery applications. Different polymer materials submerged in nanobubble dispersions exhibited varied effects on NB number concentrations due to hydrophobic interactions. In-vivo studies in Wistar rats revealed gradual drug release from the formulation, leading to an increased time to reach maximum concentration (Tmax). These findings indicated a significant improvement in the oral bioavailability of the chosen medicine using nanobubbles compared to free drug. The improved bioavailability of nanobubbles with PLGA is achieved through various mechanisms. These include better drug encapsulation within PLGA nanoparticles, longer circulation time due to the protective coating of PLGA, and increased uptake by target cells or tissues32.

As a result, these mechanisms contribute to enhanced therapeutic outcomes.

5. CONCLUSION

This research introduces an innovative approach to improving the solubility of enzalutamide (ENZ) nanobubbles. By conducting a thorough investigation, the study demonstrates that nanobubbles significantly enhance the release of drug, indicating their potential as a new and smart delivery system. Response surface methodology ensures precise control over the size distribution, resulting in improved uniformity. Additionally, drug-loaded nanobubbles exhibit exceptional stability and dissolution in the gastrointestinal tract compared to traditional drug suspensions, suggesting a longer drug half-life and increased effectiveness. These findings highlight the promising role of PLGA nanobubbles in ultrasound-responsive formulations for cancer therapy, offering notable benefits such as faster dissolution rates, sustained, targeted drug release, and improved oral bioavailability.

CONFLICT OF INTEREST

None

REFERENCES

1. Culp MBB, Soerjomataram I, Efstathiou JA, Bray F, Jemal A. Recent Global Patterns in Prostate Cancer Incidence and Mortality Rates. Eur Urol. 2020;77(1):38-52. doi:10.1016/j.eururo.2019.08.005

2. Hariharan K, Padmanabha V. Demography and disease characteristics of prostate cancer in India. Indian J Urol. 2016;32(2):103-108. doi:10.4103/0970-1591.174774

3. Siddiqui ZA, Krauss DJ. Adjuvant androgen deprivation therapy for prostate cancer treated with radiation therapy. Transl Androl Urol. 2018;7(3):378-389. doi:10.21037/tau.2018.01.06

4. Hughes DL. Review of Synthetic Routes and Crystalline Forms of the Oncology Drugs Capmatinib, Selpercatinib, and Pralsetinib. Org Process Res Dev. 2021;25(10):2192-2204. doi:10.1021/acs.oprd.1c00282

5. Mori K, Mostafaei H, Pradere B, et al. Apalutamide, enzalutamide, and darolutamide for non-metastatic castration-resistant prostate cancer: a systematic review and network meta-analysis. Int J Clin Oncol. 2020;25(11):1892-1900. doi:10.1007/s10147-020-01777-9

6. Beer TM, Armstrong AJ, Rathkopf DE, et al. Enzalutamide in Metastatic Prostate Cancer before Chemotherapy. N Engl J Med. 2014;371(5):424-433. doi:10.1056/nejmoa1405095

7. Hussain M, Fizazi K, Saad F, et al. Enzalutamide in Men with Nonmetastatic, Castration-Resistant Prostate Cancer. N Engl J Med. 2018;378(26):2465-2474. doi:10.1056/nejmoa1800536

8. Scher HI, Fizazi K, Saad F, et al. Increased Survival with Enzalutamide in Prostate Cancer after Chemotherapy. N Engl J Med. 2012;367(13):1187-1197. doi:10.1056/nejmoa1207506

9. Ning YM, Pierce W, Maher VE, et al. Enzalutamide for treatment of patients with metastatic castration-resistant prostate cancer who have previously received docetaxel: U.S. foodand drugadministrationdrug approval summary. Clin Cancer Res. 2013;19(22):6067-6073. doi:10.1158/1078-0432.CCR-13-1763

10. Rice MA, Malhotra S V., Stoyanova T. Second-generation antiandrogens: From discovery to standard of care in castration resistant prostate cancer. Front Neurol. 2019;10(AUG):801. doi:10.3389/fonc.2019.00801

11. Guo X, Guo Y, Zhang M, et al. A comparative study on in vitro and in vivo characteristics of enzalutamide nanocrystals versus amorphous solid dispersions and a better prediction for bioavailability based on “spring-parachute” model. Int J Pharm. 2022;628. doi:10.1016/j.ijpharm.2022.122333

12. Lee SM, Lee JG, Yun TH, Cho JH, Kim KS. Enhanced Stability and Improved Oral Absorption of Enzalutamide with Self-Nanoemulsifying Drug Delivery System. Int J Mol Sci. 2024;25(2). doi:10.3390/ijms25021197

13. Lee SM;, Lee JG;, Yun TH;, et al. The Impact of Polymers on Enzalutamide Solid Self-Nanoemulsifying Drug Delivery System and Improved Bioavailability. Pharm 2024, Vol 16, Page 457. 2024;16(4):457. doi:10.3390/PHARMACEUTICS16040457

14. Pavithra K, Bhagawati ST, Manjunath K. Development and evaluation of tizanidine hydrochloride loaded solid lipid nanoparticles. Asian J Pharm Clin Res. 2019;10(2):152-158. doi:10.22159/ajpcr.2019.v12i10.34545

15. Foudas AW, Kosheleva RI, Favvas EP, Kostoglou M, Mitropoulos AC, Kyzas GZ. Fundamentals and applications of nanobubbles: A review. Chem Eng Res Des. 2023;189:64-86. doi:10.1016/j.cherd.2022.11.013

16. Wang Y, Wang T. Preparation Method and Application of Nanobubbles: A Review. Coatings. 2023;13(9):1510. doi:10.3390/coatings13091510

17. Puszkiel A, Plé A, Huillard O, et al. A simple HPLC-UV method for quantification of enzalutamide and its active metabolite N-desmethyl enzalutamide in patients with metastatic castration-resistant prostate cancer. J Chromatogr B Anal Technol Biomed Life Sci. 2017;1058:102-107. doi:10.1016/j.jchromb.2017.04.014Gao J, Liu J, Meng Z, et al. Ultrasound-assisted C3F8-filled PLGA nanobubbles for enhanced FGF21 delivery and improved prophylactic treatment of diabetic cardiomyopathy. Acta Biomater. 2021;130:395-408. doi:10.1016/j.actbio.2021.06.015

18. Ponnaganti M, Kishore Babu A. Preparation, Characterization And Evaluation Of Chitosan Nanobubbles For The Targeted Delivery Of Ibrutinib. Vol 8.; 2021. Accessed April 9, 2024. https://www.nveo.org/index.php/journal/article/view/4379

19. Sampathi S, Amancha R, Dodoala SD, Kuchana V. Biodegradable polymeric nanocarriers for oral delivery of antiretroviral drug: Pharmacokinetic and in vitro permeability studies. J Appl Pharm Sci. 2021;11(4):028-039. doi:10.7324/JAPS.2021.110405

20. Rangaraj N, Pailla SR, Chowta P, Sampathi S. Fabrication of Ibrutinib Nanosuspension by Quality by Design Approach: Intended for Enhanced Oral Bioavailability and Diminished Fast Fed Variability. AAPS PharmSciTech. 2019;20(8). doi:10.1208/s12249-019-1524-7

21. Hernandez C, Abenojar EC, Hadley J, et al. Sink or float? Characterization of shell-stabilized bulk nanobubbles using a resonant mass measurement technique. Nanoscale. 2019;11(3):851-855. doi:10.1039/c8nr08763f

22. Su C, Ren XJ, Nie F, et al. Current advances in ultrasound-combined nanobubbles for cancer-targeted therapy: a review of the current status and future perspectives. RSC Adv. 2021;11(21):12915-12928. doi:10.1039/d0ra08727k

23. Burgess MT, Porter TM. Control of Acoustic Cavitation for Efficient Sonoporation with Phase-Shift Nanoemulsions. Ultrasound Med Biol. 2019;45(3):846-858. doi:10.1016/j.ultrasmedbio.2018.12.001

24. Kripfgans OD, Fabiilli ML, Carson PL, Fowlkes JB. On the acoustic vaporization of micrometer-sized droplets. J Acoust Soc Am. 2004;116(1):272-281. doi:10.1121/1.1755236

25. Kyzas GZ, Mitropoulos AC. From bubbles to nanobubbles. Nanomaterials. 2021;11(10):2592. doi:10.3390/nano11102592

26. Danaei M, Dehghankhold M, Ataei S, et al. Impact of particle size and polydispersity index on the clinical applications of lipidic nanocarrier systems. Pharmaceutics. 2018;10(2). doi:10.3390/pharmaceutics10020057

27. Bessone F, Argenziano M, Grillo G, et al. Low-dose curcuminoid-loaded in dextran nanobubbles can prevent metastatic spreading in prostate cancer cells. Nanotechnology. 2019;30(21). doi:10.1088/1361-6528/aaff96

28. Makadia HK, Siegel SJ. Poly Lactic-co-Glycolic Acid (PLGA) as biodegradable controlled drug delivery carrier. Polymers (Basel). 2011;3(3):1377-1397. doi:10.3390/polym3031377

29. Wiśniewska M, Ostolska I, Szewczuk-Karpisz K, et al. Investigation of the polyvinyl alcohol stabilization mechanism and adsorption properties on the surface of ternary mixed nanooxide AST 50 (Al2O3–SiO2–TiO2). J Nanoparticle Res. 2015;17(1). doi:10.1007/s11051-014-2831-2

30. Michailidi ED, Bomis G, Varoutoglou A, et al. Bulk nanobubbles: Production and investigation of their formation/stability mechanism. J Colloid Interface Sci. 2020;564(5):371-380. doi:10.1016/j.jcis.2019.12.093

31. Jin J, Yang L, Chen F, Gu N. Drug delivery system based on nanobubbles. Interdiscip Mater. 2022;1(4):471-494. doi:10.1002/idm2.12050.

Supplementary data:

Supplementary table 1: FTIR spectral data with wave number and the corresponding groups

Wave number (cm^{-1})	**Corresponding group in pure drug**	**Wave number (cm^{-1})**	**Corresponding group in pure drug**
3433	O-H stretching, typical in alcohols and phenols	1136	C-N stretching (amine or amide groups)
3095	C-H stretching(alkyl or aromatic groups)	998	C-H bending, likely from alkyl groups
2951	C-H stretching from alkyl groups	786	C-H bending (alkyl groups)
2233	C≡N	**Wave number (cm^{-1})**	**Corresponding group in PLGA**
1763	C=O stretching	3455	OH end group
1270	C-O stretching, typically found in ethers or esters.	2886	C-H stretch
1607	C=C stretching	1762	C=O stretch
1499	C=C stretching in aromatic rings	1186	C-O stretch
		1455	C-H bends